Probing Inhomogeneous Vibrational Reorganization Energy Barriers of Interfacial Electron Transfer

Duohai Pan, Dehong Hu, and H. Peter Lu*

Pacific Northwest National Laboratory, Fundamental Science Division, Richland, Washington 99352

Received: February 8, 2005

An atomic force microscopy (AFM) and confocal Raman microscopy study of the interfacial electron transfer of a dye-sensitization system, i.e., alizarin adsorbed upon TiO_2 nanoparticles, has revealed the distribution of the mode-specific vibrational reorganization energies encompassing different local sites (∼250-nm spatial resolution). Our experimental results suggest inhomogeneous vibrational reorganization energy barriers and different Franck−Condon coupling factors of the interfacial electron transfer. The total vibrational reorganization energy was inhomogeneous from site to site; specifically, mode-specific analyses indicated that energy distributions were inhomogeneous for bridging normal modes and less inhomogeneous or homogeneous for nonbridging normal modes, especially for modes far away from the alizarin−TiO_2 coupling hydroxyl modes. The results demonstrate a significant step forward in characterizing site-specific inhomogeneous interfacial charge-transfer dynamics.

Introduction

Interfacial electron-transfer processes in dye-sensitized semiconductor systems often involve complex and inhomogeneous dynamics.[1−11] The complexity and inhomogeneity come from the spatial heterogeneities of the surfaces and the inhomogeneous vibronic coupling between the adsorbed molecules and the nanoscale rough surfaces of the substrates.[12−14] There have been extensive studies of interfacial electron-transfer dynamics in dye-sensitized semiconductor nanoparticles and thin films by ultrafast time-resolved spectroscopy, such as transient absorption and fluorescence lifetime measurement, in the visible and near-IR regions,[2,3,5,6,9−11] which provided much insight regarding interfacial electron-transfer dynamics. Moreover, resonance Raman spectroscopy approaches have been powerful in characterizing vibrational Franck−Condon coupling barriers of interfacial electron-transfer reactions.[15−20] For example, this technique has been applied to determine vibrational reorganization energies for charge transfer in dye-sensitized TiO_2 nanoparticles.[17] However, our knowledge of the spatial and temporal inhomogeneities of interfacial electron-transfer dynamics[4,7,8] is inadequate to characterize the heterogeneous local environments of nanoparticles and the nanoscale roughness on the surfaces of the substrates. Interfacial electron-transfer dynamics can be different from site to site and from time to time[4,7,8] and can involve both static and dynamic inhomogeneities.[21] Presumably, the inhomogeneity and fluctuations of the local driving force, the vibrational reorganization energy, the solvent reorganization energy, the electronic and Franck−Condon couplings, and the electron trapping and scattering at the interfaces and in the bulk of the semiconductor substrates could all contribute to the complexity and inhomogeneity in interfacial electron-transfer dynamics.[1−14]

It is desirable to obtain a correlated topographic and spectroscopic characterization with high chemical sensitivity, high spatial resolution, and spectroscopic selectivity for electron-transfer systems. Specifically, a characterization of site-specific vibrational coupling and reorganization energy is critical for a fundamental understanding of the complexity and inhomogeneity of the dynamics of interfacial electron transfer. However, to date, a nanoscale site-specific vibrational reorganization energy characterization of interfacial electron-transfer dynamics has yet to be achieved. Consequently, to our knowledge, the possible inhomogeneity of the mode-specific vibrational reorganization energy of interfacial electron transfer has not been experimentally demonstrated and analyzed.

In this paper, we report on a study that used both resonance Raman microscopy and atomic force microscopy (AFM) to characterize the vibrational reorganization energy barriers of the interfacial electron transfer in a dye-sensitization system, namely, alizarin adsorbed on TiO_2 nanoparticles.[22,23] We observed that the Raman peak intensity and peak-to-peak intensity ratio are different among different submicrometer-scale spots at the TiO_2 nanoparticle layer. We then focused on revealing inhomogeneous vibrational reorganization energy barriers for interfacial electron transfer, using a time-dependent wave packet propagation analysis of resonance Raman spectra[15−19] to obtain mode-specific vibrational reorganization energies upon the charge-transfer reactions for individual spots under a ∼250-nm spatial resolution. Although the spatial resolution of our Raman spectroscopy was not at nanoscale, nonetheless our results present a significant step forward in characterizing site-specific vibrational reorganization energy and shed light on inhomogeneous interfacial electron-transfer dynamics in terms of inhomogeneous Franck−Condon barriers.

Experimental Section

The colloid TiO_2 solution at pH 3 with a TiO_2 content of 500 mg/L was prepared by the hydrolysis of titanium isopropoxide.[22] The average diameter of the TiO_2 nanoparticles was ∼12 nm.[7] The TiO_2−alizarin nanoparticle charge-transfer complex was prepared by slowly adding the alizarin solution (0.5 mM) into vigorously stirred colloidal TiO_2 in water.

* Corresponding author. Email: peter.lu@pnl.gov. Phone: 509-376-3897. Fax: 509-376-6066.

10.1021/jp058043v CCC: $30.25
Published on Web 07/28/2005

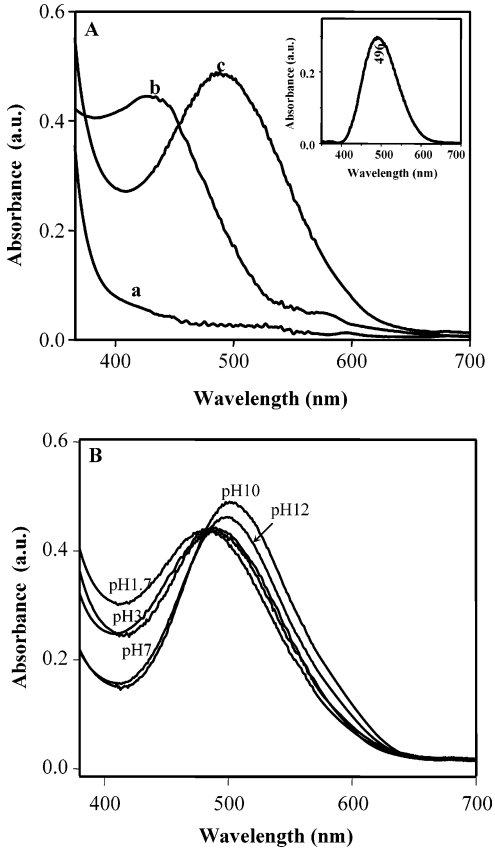

Figure 1. (A) Absorption spectra of alizarin/TiO_2 system. Absorption spectra of TiO_2 (a), alizarin alone (b), and alizarin/TiO_2 complex (c) in aqueous solution at pH 3. The insert shows the charge-transfer associated excitation band at 496 nm, which was obtained by subtracting alizarin-alone and TiO_2 spectra from the spectrum of alizarin adsorbed on the TiO_2 nanoparticles. (B) Absorption spectra of alizarin/TiO_2 under pH ranging from 1.7 to 12. It is evident that the absorption band at 496 nm is pH-independent at pH < 7.

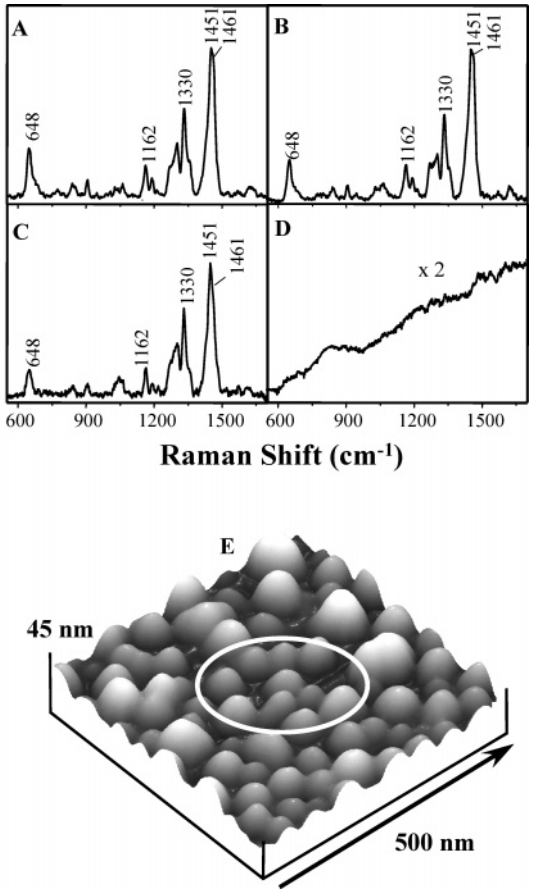

Figure 2. Resonance Raman and AFM characterization of alizarin/TiO_2 interfacial electron transfer. (A) Resonance microscopic Raman spectrum of the alizarin/TiO_2 complex with a monolayer on a thin silver film was obtained by 514.5-nm excitation. A 20-μL alizarin (0.05-mM) and TiO_2 solution at pH 3 was spin-coated on a thin silver film. (B) and (C) Resonance Raman spectra of the alizarin/TiO_2 complex for two different spots. (D) Raman spectrum of alizarin alone (0.05 mM) adsorbed on a thin silver film. (E) An AFM image of the microscopic site, mostly nanoparticle clusters. The marked part in the AFM image corresponds to the spot where the Raman spectrum (A) was collected. It was estimated that ~2000 alizarin molecules were at a single nanoparticle.

Details of the experimental setup have been published elsewhere.[24−26] Briefly, a confocal Raman imaging microscope combined with an AFM microscope was used for topographic and spectroscopic measurements. A 514.5-nm laser beam was reflected by a dichroic beam splitter (530 dclp, Chroma Technology Corp.) and focused by a high numerical aperture objective (1.4 NA, 63 X, Zeiss) on the sample surface. The alizarin-sensitized TiO_2 nanoparticles were spin-cast on a cover glass that was precoated with a thin silver film (~10 nm thick), which provided an electromagnetic field enhancement for the Raman scattering.[27] The Raman band frequencies (Figure 2A) were identical to those of the alizarin/TiO_2 complex in solution phase, indicating that there was no surface perturbation of the enhanced Raman signals associated with interfacial electron transfer.[28] The AFM probe (Nanoscope III microscope, Veeco Metrology) was aligned with the laser focal spot by correlating the fluorescence intensity image and the AFM tip light-scattering pattern.[24−26] The tapping-mode AFM imaging was used to characterize the topographic features of the individual microscopic spots. Raman signals were collected with the same objective and detected by using a N_2-cooled CCD (Spec-10: 400 BR (LN), Roper Scientific, Inc.) coupled to a spectrometer (Holespec f/1.8i, Kaiser Optical System, Inc.). Raman spectra were corrected for the wavelength dependence of the spectrometer efficiency by using white light and were calibrated with a mercury lamp.

Raman and Absorption Spectral Analysis. The resonance Raman and absorption cross-sections were calculated using the following time-dependent wave packet propagation formalism:[15−19]

$$\sigma_{R,i\to f}(\omega_L) = \frac{8\pi(eM)^4\omega_L\omega_S^3}{9\hbar^2c^4}\sum_i P_i\left|\int_0^\infty dt\langle f|i(t)\rangle \exp[i(\omega_L+\omega_i-\omega_0)t-\gamma t/2]\right|^2 \quad (1)$$

$$\sigma_A(\omega) = \frac{4\pi(eM)^2\omega}{3\hbar c}\sum_i P_i\,\mathrm{Re}\int_0^\infty dt\langle i|i(t)\rangle \exp[i(\omega+\omega_i-\omega_0)t-\gamma t/2]\Big|^2 \quad (2)$$

where ω_L and ω_s are the incident (laser) and scattered photon frequencies, respectively; eM is the electronic transition dipole moment; $|i\rangle$ and $|f\rangle$ are the initial and final vibrational states on the ground-state potential energy surface, respectively; P_i is the Boltzmann population of initial vibrational state; ω_i is the vibrational frequency at the vibrational level of $|i\rangle$ or $|f\rangle$; ω_0 is the electronic zero−zero energy; γ is the inverse lifetime of the excited state; and $|i(t)\rangle$ is the vibrational wave packet function propagating in time t on the excited-state potential

surface. In our treatment, the $\langle i|i(t)\rangle$ and $\langle f|i(t)\rangle$ overlaps are dependent on the displacement, Δ, in dimensionless normal coordinates between ground- and excited-state equilibrium geometries along each normal coordinate. The initial guesses for Δ were given from the relative resonance Raman intensities, assuming that the intensity ratios were proportional to $\Delta^2\nu^2$ ratios, where ν is the vibrational frequency.[15−19] The homogeneous broadening (Γ) was calculated from the homogeneous line width function.[19] The inhomogeneous broadening (Φ), a standard deviation of the normalized inhomogeneous Gaussian distribution function, was determined by the absorption bandshape and resonance Raman intensity.[19] The energy gap between potential surfaces, ω_0, was initially determined by the wavelength of the absorption spectrum maximum arising from the electron-transfer reaction. The parameters were optimized iteratively until the calculated and experimental absorption spectrum and resonance Raman intensities were in agreement. Finally, the mode-specific reorganization energy (λ_ν), assuming the vibrations to be harmonic, was calculated by[15−19]

$$\lambda_\nu = \frac{1}{2}\nu\Delta^2 \tag{3}$$

Results and Discussion

Figure 1 shows the absorption spectra of TiO_2, alizarin-alone, and alizarin/TiO_2 complex in aqueous solution at pH 3. The strong electron-transfer band at 496 nm with a molar absorption coefficient of 8660 $M^{-1}cm^{-1}$ (Figure 1, inset) formed when alizarin was adsorbed on the TiO_2 nanoparticle surface. The 65-nm red shift from 431 nm of the alizarin-alone absorption spectrum to 496 nm of the spectrum upon alizarin/TiO_2 adsorption was due to charge-transfer interaction between alizarin and the nanoparticle surface.[23] Examining the pH dependence of the absorption band, we confirmed that the 496-nm absorption band was pH-independent in the range of pH 3−7 (Figure 1B), as previously reported in the literature.[30] At higher pH values, TiO_2 nanoparticles were readily precipitated, and the absorption band under pH 10 presumably resulted from the pH-dependent absorption of deprotonated alizarin. The result of the pH independence in a wide range further confirms that the 496-nm band was associated with a strong charge-transfer interaction.[30,31] Furthermore, alizarin fluorescence was completely quenched in the alizarin/TiO_2 system, which strongly suggests an electron-transfer interaction between adsorbed alizarin and the TiO_2 nanoparticles. We have also measured the absorption spectra of deprotonated alizarin in solution at pH 7−12, and the absorption band maximum ranged from 526 to 535 nm (data not shown), significantly red-shifted from the absorption peak of 496 nm in the alizarin/TiO_2 system. Under laser excitation at 514.5 nm, both the interfacial electron-transfer state and the Raman-normal coordinate modes that involve electron transfer under this absorption band were resonantly excited simultaneously. Therefore, we were able to identify and selectively measure the electron transfer associated with Raman-normal modes, i.e., the electron-transfer Franck−Condon activation-contributing vibrational modes. We then obtained the vibrational reorganization energy for each of these vibrational modes using time-dependent wave packet analysis of the absorption and Raman spectra of the alizarin/TiO_2 electron-transfer system.[17−19]

Correlated AFM images were obtained for the microscopic Raman spectral collection at optical diffraction-limited imaging sites. Figure 2A−C shows the resonance Raman spectra of the alizarin/TiO_2 complex for three different spots (~250 nm)

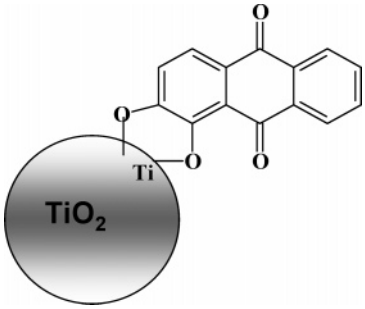

Figure 3. Sketch of alizarin/TiO_2 nanoparticle surface adsorption of alizarin via the hydroxyl group bonding to the TiO_2 nanoparticles.

consisting of TiO_2 nanoparticle clusters. In contrast, because of the high fluorescence background and off-resonant excitation, no Raman bands were detected from an alizarin-alone sample under the same experimental conditions (Figure 2D), because there were no contributions from the electron-transfer resonance Raman enhancement.[29] This observation supports our conclusion that the enhanced Raman signals in Figure 2A−C were associated with interfacial electron transfer from the excited state of the alizarin to the TiO_2 nanoparticles. Moreover, the Raman peak intensities (Figure 2A−C) were significantly different from those reported in the literature[29] of peak intensities for free alizarin molecules obtained with excitation near UV levels. This suggests that the Raman scattering was predominately from the enhanced Raman modes associated with charge-transfer resonant excitation. The AFM image in Figure 2E provides topographic features of the TiO_2 nanoparticle clusters on the microscopic sites where the Raman spectrum (Figure 2A) was collected.

The resonance Raman spectra in the alizarin/TiO_2 complex (Figure 2A−C) exhibited 20 vibrational bands.[29] The most prominent bands, at 1451 and 1461 cm^{-1}, were assigned to the ring C═C stretches.[29] The C−O stretch combined with the ring C═C stretch mode corresponds to the intense bands at 1330 cm^{-1} and in the region 1268−1300 cm^{-1} (Figure 2A−C). The 648 cm^{-1} band was attributable to a Ti−O stretching mode from a bridging Ti−O−C bond.[32] In comparison to the free molecules, the increased Raman intensity in the C−O stretching at 1330 cm^{-1} revealed that the hydroxyl groups provided the primary bridging bonds to the interfacial charge transfer (Figure 3). In addition, no resonance enhancement of TiO_2 vibrational bands below 500 cm^{-1} was detected for this charge-transfer complex in our measurements.

It is revealing that the peak-to-peak Raman intensity ratios were significantly different among the Raman spectra from different sites (Figure 2A−C). For example, the intensity ratios of 648 cm^{-1} to 1162 cm^{-1} in Figure 2A, B, and C are 1.8, 1.6, and 1.1, respectively. Our resonance Raman measurements showed good signal-to-noise ratios (>100:1) for these two peaks. However, the ratio changes of these Raman peak intensities are far beyond the measurement error. Presumably, the changes indicate the existence of an inhomogeneity in the vibrational reorganization energy. To specify and characterize such an inhomogeneity, we used the time-dependent wave packet calculations to analyze correlatively the Raman and absorption spectra, obtaining the vibrational reorganization energy of individual normal modes of the alizarin/TiO_2 complex under interfacial charge-transfer reaction at each microscopic site. The resonance Raman intensities, especially for the ultrafast process with less than 10 fs forward electron ejection time from the excited state of the alizarin,[11] reflected the conformational distortion of the molecule along the measured normal modes associated with charge-transfer excitation.[29]

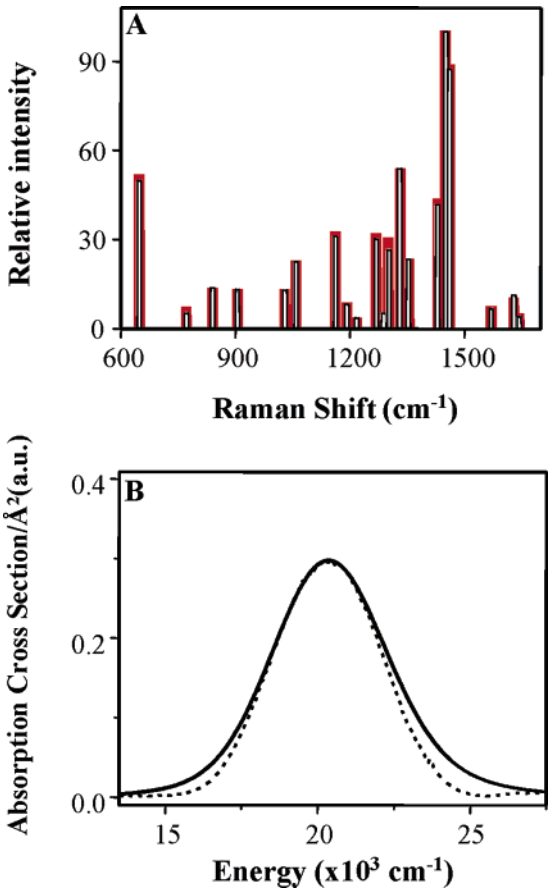

Figure 4. Time-dependent wave packet analysis of Raman and absorption spectra. (A) Comparison of experimental (white) and calculated (red) resonance Raman intensities of all observed modes for a specific microscopic site. (B) The absorption cross-section of experimental (solid) and calculated (dotted) charge transfer associated excitation bands of the alizarin/TiO_2 complex in solution.

We analyzed the resonance Raman cross-sections, the charge-transfer absorption spectrum (to determine the spectral broadening and Raman damping parameters), and the electronic transition energy. The analysis provided detailed information about changes in nuclear equilibrium geometry for both the electron donor−acceptor and the surrounding local environment in the interfacial charge-transfer processes. Figure 4A shows a typical fitting of the experimental Raman intensities for the observed Raman peaks from a specific spot (Figure 2E). Figure 4B presents the corresponding experimental and fitting absorption spectral band at 496 nm, a strong charge-transfer interaction band.[23] The model generates a good fit to both the relative intensities of the Raman peaks and the charge-transfer absorption spectrum with the parameters of electronic zero−zero energy ($\omega_0 = 20\,010$ cm^{-1}), homogeneous broadening ($\Gamma = 550$ cm^{-1}), inhomogeneous broadening ($\Phi = 1600$ cm^{-1}), and frequencies and intensities of the 20 resonant Raman modes.[33] From the time-dependent wave packet analysis of the Raman and absorption spectra, we obtained unitless normal-coordinate displacements, Δ, for each electron-transfer associated resonant Raman mode. The vibrational reorganization energies along each of the observed Raman modes were calculated from the unitless normal-coordinate displacement by using eq 3.[15−19] Although the calculated results here are based on the Raman data from a single excitation wavelength, instead of a Raman excitation profile and using an internal standard for the absolute Raman cross-sections,[29] the electron-transfer excited vibrational modes were representative, since the charge-transfer interaction resonant band of the alizarin/TiO_2 complex clearly contained a single electronic transition.[29] Our spectral analysis yielded a total vibrational reorganization energy of 0.045 eV for this specific spot (Figure 2E), which is consistent with the result obtained from the ensemble-averaged Raman excitation profile.[29] The experimental and calculated resonance Raman parameters for this specific spot are shown in Table 1. The bands of C−O and Ti−O stretching modes account for ∼30% of the total internal reorganization energy, which suggests that electron donation from alizarin to the TiO_2 nanoparticles along the hydroxyl groups is strongly coupled to interfacial electron transfer. This result agrees with molecular orbital calculations that the strong electronic coupling occurs through the two hydroxyl groups to one surface Ti^{4+} ion.[23]

TABLE 1: Experimental and Calculated Parameters and Vibrational Band Assignments[a]

ν (cm^{-1})	Δ	λ_ν (cm^{-1})	assignment[b]
648	0.294	28	skeletal + TiO_2 stretch
773	0.12	5.55	out-of-plane OH + skeletal
837	0.145	8.83	skeletal
906	0.117	6.19	in-plane CH bend
1031	0.103	5.46	in-plane CH bend
1059	0.11	6.4	in-plane CH bend
1162	0.171	17	in-plane CH bend
1191	0.101	6.1	in-plane CH bend
1217	0.085	4.4	C−O stretch + ring stretch
1268	0.14	12.4	ring stretch + C−O stretch
1288	0.168	18.2	C−O stretch + ring stretch
1301	0.151	14.8	C−O stretch + ring stretch
1330	0.28	52.1	C−O stretch + ring stretch
1357	0.137	12.7	ring stretch
1431	0.179	22.9	ring stretch
1451	0.301	65.7	ring stretch
1461	0.298	64.9	ring stretch
1570	0.067	3.52	ring stretch
1629	0.7	3.99	C═O stretch
1646	0.065	3.48	C═O stretch
		$\lambda_{total} = 366$ cm^{-1} (0.045 eV)	

[a] Other parameters: zero−zero energy $\omega_0 = 20\,010$ cm^{-1}, $\Gamma = 550$ cm^{-1}, $\Phi = 1600$ cm^{-1}. [b] See ref 29.

The most significant finding from our experiments is that the vibrational reorganization energy is inhomogeneous, i.e., different from microscopic site to site of this alizarin/TiO_2 interfacial electron-transfer system. Correlating the topographic AFM imaging, we measured the resonance Raman spectra at different microscopic spots and found that relative Raman intensities of the Ti−O, C−O, and ring stretching modes were significantly different from site to site (Figure 2A, B, and C). These relative Raman intensity changes presumably resulted from properties intrinsic to interfacial charge transfer.[12−19] Different Raman normal-mode intensities would give different unitless displacements and, therefore, different vibrational reorganization energies (see eq 3). Figure 5A, B, and C shows, respectively, the distributions of the Ti−O stretching mode, the C−O stretching mode, and the ring C═C stretching mode reorganization energies among the measured individual sites. The reorganization energy for the C−O bridge mode changes was measured from 63 to 97 cm^{-1}; the Ti−O bridge mode gave measurable vibration reorganization energy from 12 to 28 cm^{-1}; and the ring C═C stretching mode yielded a range from 30 to 65 cm^{-1}. Consequently, the total vibrational reorganization energy, λ_{total}, was obtained from values between 242 and 380 cm^{-1} (Figure 5D). The λ_{total} was predominately contributed from the bridging modes at the alizarin/TiO_2 interface. Since the unitless normal-coordinate displacement was ultimately constrained by other parameters, such as the amplitudes, bandwidth, and band shape of the absorption spectrum and resonance

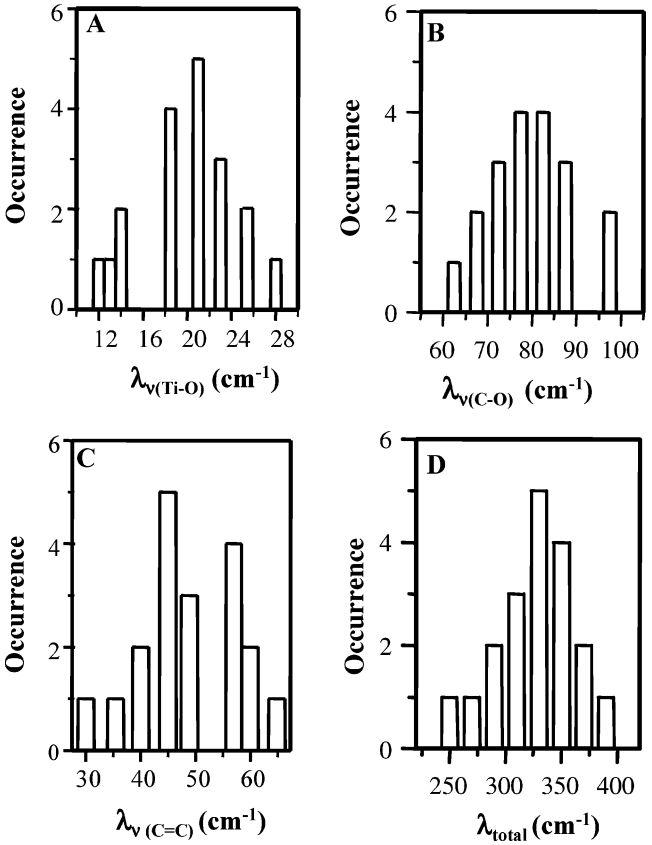

Figure 5. Distributions of the vibrational reorganization energy for (A) Ti−O stretch, (B) C−O stretch, (C) ring C═C stretch, and (D) total modes at a number of individual microscopic sites. The standard deviations of the mode-specific displacements were ±4 cm^{-1} for Ti−O stretch and ±5 cm^{-1} for both C−O and ring C═C stretches. The width of the distributions is beyond the measurement error bar and attributed to the inhomogeneity of the vibrational reorganization energy from site to site of the interfacial electron transfer.

Raman intensity, our measurement error for the total vibrational reorganization energy was about 30 cm^{-1}, which was significantly smaller that the distribution bandwidth of 90 cm^{-1}.[34]

The distribution of the vibrational reorganization energies suggests that each specific site may have had a different locally averaged vibronic interaction and a different mode-specific Franck−Condon coupling factor for the interfacial electron-transfer process. Since the forward electron-transfer rate in the alizarin/TiO_2 complex was less than 100 fs,[23] or even possibly less than 10 fs,[11] due to the strong vibronic coupling and high density of states in TiO_2, the ultrafast interfacial electron transfer was comparable to the Raman excitation wave packet relaxation of the adsorbed molecule. It has been proposed that the small observed reorganization energy for the alizarin/TiO_2 complex would arise from rapid electronic and vibrational dephasing, which would effectively dampen out the vibrational-mode Raman excitation of TiO_2 or even the alizarin.[29]

We observed that not all of the vibrational modes associated with electron transfer had inhomogeneous energies. The vibrational reorganization energy distributions of the specific normal modes in the alizarin/TiO_2 complex were homogeneous for those modes located away from direct binding with the TiO_2. For example, Figure 6A and B shows the vibrational reorganization energy distributions of two C−H in-plane bending modes, revealing the distributions to be within the measurement error bars and significantly narrower than distributions of bridging modes (compare to Figure 5A and B). However, since 70% of the overall vibrational reorganization energy was contributed

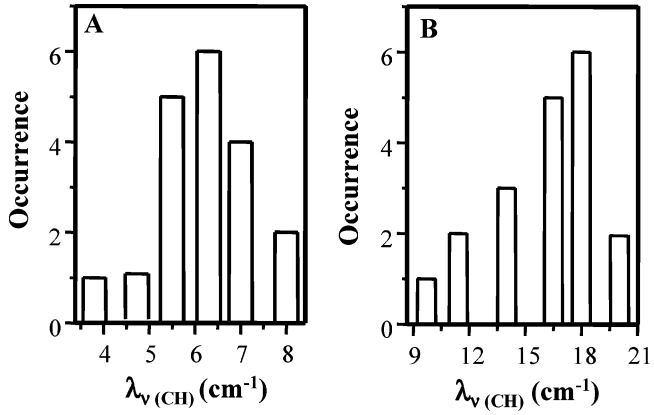

Figure 6. Distributions of reorganization energies for the C−H in-plane bending modes at 1162 cm^{-1} (A) and 1191 cm^{-1} (B) at a number of individual microscopic sites. Evidentially, the broadness of the distribution is not beyond the measurement error bars of ±4 cm^{-1}, i.e., there was no inhomogeneity observed.

from the bridging modes, the overall vibrational reorganization energy was nevertheless inhomogeneous. The high specificity of AFM−Raman spectroscopy provided the capability of revealing inhomogeneous vibrational reorganization energies of the interfacial electron transfer associated with the heterogeneous local environment and the chemical interactions at the alizarin−TiO_2 interfaces.

Technically, it is difficult to measure excitation spectra under various excitation wavelengths at each microscopic site examined. We used the ensemble-averaged absorption spectrum from the alizarin/TiO_2 complexes for the site-specific spectral analysis because, as demonstrated in the literature,[29] the electron transfer band excitation is a single electron transition excitation. It is also technically complicated to use internal standard molecules to obtain site-specific absolute Raman cross-section calculations. In addition, the possible contribution of solvent reorganization energy to total reorganization energy has been accounted for in our spectral analysis by analyzing the absorption bandwidth of homogeneous broadening.[29,35] Nevertheless, the mean total vibrational reorganization energy distribution is consistent with the result of the ensemble-averaged measurements in the solution phase.[29]

The focus of this work is to reveal the inhomogeneous distributions of the vibrational reorganization energy, and our microscopic approach has, for the first time to the best of our knowledge, experimentally demonstrated the existence of inhomogeneity. At a spatial resolution of ∼250 nm, our microscopic Raman spectra were still averaged results from thousands of molecules at the interfacial sites, and it is most likely that the real inhomogeneity of the vibrational reorganization energy was even larger at a single-molecule level or at nanoscale measurements. Obviously, further study is needed to achieve higher spatial resolution and spectral sensitivity in order to obtain nanoscale site-specific characterization of the inhomogeneous vibrational reorganization energy barriers.

The most-needed technical and scientific advances include the following: (1) AFM-tip enhanced near-field Raman spectroscopic measurements for dye-sensitized semiconductor nanoparticles,[36−46] (2) higher measurement sensitivity to measure a small number of molecules or even single molecules at nanoscale sites, and (3) a molecular-level understanding of the relationship between topographical nanoscale structures and surface chemical bounding structures. Nevertheless, by experimentally observing the existence of an inhomogeneity in the vibrational reorganization energy barrier, we have made a step

forward to achieving a greater understanding of the complex interfacial electron-transfer dynamics. This inhomogeneity may well contribute to the inhomogeneous interfacial electron-transfer dynamics observed in this and other interfacial electron-transfer dye/TiO_2 systems reported in the literature.[2,3,9,14] It is also notable that various factors, such as driving force, the density of states in the semiconductor, electron trapping, and scattering in a back electron-transfer process, would contribute to the inhomogeneous interfacial electron-transfer dynamics.[2,47] However, characterizing all these critical parameters in the alizarin−TiO_2 system is beyond the scope of this work.

Conclusions

Applying a microscopic AFM−Raman characterization and analysis, we revealed that, for alizarin/TiO_2 interfaces, the vibrational reorganization energy barriers of interfacial electron transfer are inhomogeneous at a sub-mesoscale (~250 nm). We found that (1) the total vibrational reorganization energy was inhomogeneous from site to site, (2) the alizarin/TiO_2 bridging normal modes were the primary contributor to the total vibrational reorganization energy and its inhomogeneity, (3) the mode-specific analyses indicated that the energy distributions were inhomogeneous for bridging normal modes and less inhomogeneous or homogeneous for nonbridging normal modes, especially for modes far away from the alizarin−TiO_2 coupling hydroxyl modes, and (4) the vibrational reorganization energy inhomogeneity was closely associated with the local environmental heterogeneity of the alizarin/TiO_2 interface. It is most likely that the vibrational reorganization energy inhomogeneities contributed to the inhomogeneous dynamics of the interfacial electron-transfer processes. However, it is still a challenge to identify a detailed mechanism of the contribution of the inhomogeneity to both forward and backward electron-transfer processes in the alizarin/TiO_2 system. Although the topographic and spectroscopic detection limits reported here have not yet reached single molecules, single semiconductor nanoparticles, or even nanoscale-specific sites, our results demonstrated that correlated AFM−confocal Raman microscopy is a promising approach for a quantitative understanding of inhomogeneous interfacial charge transfers.

Acknowledgment. We thank Vasudevanpillai Biju for his technical assistance. We thank Greg Hartland, Joseph Hupp, Tim Lian, and Jeanne McHale for helpful discussions. We acknowledge our use of the spectral analysis program developed by Prof. A. M. Kelley. This work was supported by the Chemical Science Division of the Office of Basic Energy Sciences, U.S. Department of Energy (DOE). The Pacific Northwest National Laboratory is operated by Battelle for the U.S. DOE under contract DE-AC06-76RLO1830.

References and Notes

(1) Grätzel, M. *Nature (London)* **2001**, *414*, (6861), 338.
(2) Asbury, J. B.; Hao, E.; Wang, Y.; Ghosh, H. N.; Lian, T. *J. Phys. Chem. B* **2001**, *105*, 4545.
(3) Liu, D.; Kamat, P. V.; Thomas, K. G.; Thomas, K. J.; Das, S.; George, M. V. *J. Chem. Phys.* **1997**, *106*, 6404.
(4) Lu, H. P.; Xie, X. S. *J. Phys. Chem.* **1997**, *101*, 2753.
(5) Son, D. H.; Kambhampati, P.; Kee, T. W.; Barbara, P. F. *J. Phys. Chem. A* **2002**, *106*, 4591.
(6) Lu, H.; Prieskorn, J. N.; Hupp, J. T. *J. Am. Chem. Soc.* **1993**, *115*, 4927.
(7) Biju, V.; Micic, M.; Hu, D.; Lu, H. P. *J. Am. Chem. Soc.* **2004**, *112*, 9374.
(8) Holman, M. W.; Liu, R. C.; Adams, D. M. *J. Am. Chem. Soc.* **2003**, *125*, 12649.
(9) Zimmermann, C.; Willig, F.; Ramakrishna, S.; Burfeindt, B.; Pettinger, B.; Eichberger, R.; Storck, W. *J. Phys. Chem. B* **2001**, *105*, 9245.
(10) Eichberger, R.; Willig, F. *Chem. Phys.* **1990**, *141*, 159.
(11) Huber, R.; Moser, J. E.; Gratzel, M.; Wachtveitl, J. *J. Phys. Chem. B* **2002**, *106*, 6494.
(12) (a) Marcus, R. A.; Sutin, N. *Biochim. Biophys. Acta* **1985**, *811*, 265. (b) Gao, Y. Q.; Georgievskii, Y.; Marcus, R. A. *J. Chem. Phys.* **2000**, *112*, 3358.
(13) (a) Jortner, J. *J. Chem. Phys.* **1976**, *64*, 4860. (b) Van Duyne, R. P.; Fischer, S. F. *Chem Phys.* **1974**, *5*, 185.
(14) Ramakrishna, S.; Willig, F.; May, V. *J. Chem. Phys.* **2001**, *115*, 2743.
(15) Heller, E. J. *Acc. Chem. Res.* **1981**, *14*, 368.
(16) Tutt, L.; Zink, J. I. *J. Am. Chem. Soc.* **1986**, *108*, 5830.
(17) Hupp, J. T.; Williams, R. D. *Acc. Chem. Res.* **2001**, *34*, 808.
(18) Meyers, A. B.; Mathies, R. A. In *Biological Applications of Raman Spectroscopy*; Spiro, T. G., Ed.; Wiley: New York, 1988; Vol. 2, p 1.
(19) Kelley, A. M. *J. Phys. Chem. A* **1999**, *103*, 6891.
(20) Cho, M. H.; Silbey, R. J. *J. Chem. Phys.* **1995**, *103*, 595.
(21) Zwanzig, R. *Acc. Chem. Res.* **1990**, *23*, 148.
(22) (a) Duonghong, D.; Borgarell, E.; Grätzel, M, *J. Am. Chem. Soc.* **1981**, *103*, 4685. (b) O'Regan, B.; Moser, J.; Anderson, M.; Grazel, M. *J. Phys. Chem.* **1990**, *94*, 8720−8726.
(23) Huber, R.; Sporlein, S.; Moser, J. E.; Gratzel, M.; Wachtveitl, J. *J. Phys. Chem. B* **2000**, *104*, 8995.
(24) Hu, D.; Micic, M.; Klymyshyn, N.; Suh, Y. D.; Lu, H. P. *Rev. Sci. Instrum.* **2003**, *74*, 3347.
(25) Suh, Y. D.; Schenter, G. K.; Zhu, L.; Lu, H. P. *Ultramicroscopy* **2003**, *97*, 89.
(26) Hu, D.; Micic, M.; Klymyshyn, N.; Suh, Y. D.; Lu, H. P. *J. Lumin.* **2004**, *107*, 4.
(27) Moskovits, M. *Rev. Mod. Phys.* **1985**, *57*, 783.
(28) In our experiments, besides the electromagnetic field enhancement, there was no chemical enhancement from the Ag film. We observed that the Raman vibration frequencies of alizarin/TiO_2 on Ag film were identical with that in solution phase, which indicates no Ag surface perturbation to the enhanced Raman signals associated with the interfacial electron transfer at alizarin−TiO_2 interface.
(29) Shoute, L. C. T.; Loppnow, G. R. *J. Chem. Phys.* **2002**, *117*, 842.
(30) Moser, J.; Punchihewa, S.; Infelta, P. P.; Gratzel, M. *Langmuir* **1991**, *7*, 3012.
(31) Anderson, S.; Constable, E. C.; Dare-Edwards, M. P.; Goodenough, J. B.; Hamnett, A.; Seddon, K. R.; Wright, R. D. *Nature (London)* **1979**, *280*, 571.
(32) Sekiya, T.; Ohta, S.; Kamei, S.; Hanakawa, M.; Kurita, S. *J. Phys. Chem. Solids* **2001**, *62*, 717.
(33) We have assumed that the absorption spectra are essentially not site-dependent, as the spectrum is already rather broad and local inhomogeneity in absorption spectra is not experimentally detectable using conventional absorption spectral measurements.
(34) The vibrational reorganization energy is obtained from $\lambda_\nu = 0.5\nu\Delta^2$. Since the unitless displacement, Δ, is ultimately constrained by the other parameters such as the magnitudes, bandwidth, and band shape of the absorption spectrum and resonance Raman intensity, we estimate that our calculation error for the total vibrational reorganization energy is about 10%.
(35) McHale, J. L. *Acc. Chem. Res.* **2001**, *34*, 265.
(36) Micic, M.; Klymyshyn, N.; Suh, Y. D.; Lu, H. P. *J. Phys. Chem. B* **2003**, *107*, 1574.
(37) Hartschuh, A.; Sanchez, E. J.; Xie, X. S.; Novotny, L. *Phys. Rev. Lett.* **2003**, *90*, 95503.
(38) Pettinger, B.; Ren, B.; Picardi, G.; Schuster, R.; Ertl, G. *Phys. Rev. Lett.* **2004**, *92*, 096101.
(39) Gerton, J. M.; Wade, L. A.; Lessard, G. A.; Ma, Z.; Quake, S. R. *Phys. Rev. Lett.* **2004**, *93*, 180801.
(40) Bouhelier, A.; Beversluis, M. R.; Novotny, L. *Ultramicroscopy* **2004**, *100*, 413.
(41) Anger, P.; Feltz, A.; Berghaus, T.; Meixner, A. J. *J. Microsc. (Oxford, UK)* **2003**, *209*, 162.
(42) Pettinger, B.; Picardi, G.; Schuster, R.; Ertl, G. *Single Mol.* **2002**, *3*, 285.
(43) Qiu, X. H.; Nazin, G. V.; Ho, W. *Science* **2003**, *299*, 542.
(44) Hayazawa, N.; Inouye, Y.; Sekkat, Z.; Kawata, S. *J. Chem. Phys.* **2002**, *117*, 1296.
(45) Hayazawa, N.; Inouye, Y.; Sekkat, Z.; Kawata, S. *Chem. Phys. Lett.* **2001**, *335*, 369.
(46) Stockle, R. M.; Suh, Y. D.; Deckert, V.; Zenobi, R. *Chem. Phys. Lett.* **2000**, *318*, 131.
(47) Barzykin, A.V.; Tachiya, M. *J. Phys. Chem. B* **2002**, *106*, 4356.